# Malate transport by the vacuolar AtALMT6 channel in guard cells is subject to multiple regulation

Meyer, S ; Scholz-Starke, J ; De Angeli, A ; Kovermann, P ; Burla, B ; Gambale, F ; Martinoia, E

Abstract: Gas exchange in plants is controlled by guard cells, specialized cells acting as turgor pressure-driven valves. Malate is one of the major anions accumulated inside the vacuole during stomatal opening counteracting the positive charge of potassium. AtALMT6, a member of the aluminum-activated malate transporter family, is expressed in guard cells of leaves and stems as well as in flower organs of Arabidopsis thaliana. An AtALMT6-GFP fusion protein was targeted to the vacuolar membrane both in transient and stable expression systems. Patch-clamp experiments on vacuoles isolated from AtALMT6-GFP over-expressing Arabidopsis plants revealed large inward-rectifying malate currents only in the presence of micromolar cytosolic calcium concentrations. Further analyses showed that vacuolar pH and cytosolic malate regulate the threshold of activation of AtALMT6-mediated currents. The interplay of these two factors determines the AtALMT6 function as a malate influx or efflux channel depending on the tonoplast potential. Guard cell vacuoles isolated from Atalmt6 knock-out plants displayed reduced malate currents compared with wild-type vacuoles. This reduction, however, was not accompanied by phenotypic differences in the stomatal movements in knock-out plants, probably because of functional redundancy of malate transporters in guard cell vacuoles.

DOI: https://doi.org/10.1111/j.1365-313X.2011.04587.x

# Malate transport by the vacuolar AtALMT6 channel in guard cells is subject to multiple regulation

Stefan Meyer,[1,†] Joachim Scholz-Starke,[2,a,†] Alexis De Angeli,[1,*,†] Peter Kovermann,[1,b] Bo Burla,[1] Franco Gambale,[2] and Enrico Martinoia[1]

[1] Institute of Plant Biology, University of Zurich, CH-8008 Zurich, Switzerland

[2] Institute of Biophysics, National Research Council of Italy, I-16149 Genoa, Italy

[†] These authors contributed equally to this study.

[a] present address: Department of Neuroscience and Brain Technologies, Italian Institute of Technology, I-16163 Genoa, Italy

[b] present address: Institute of Neurophysiology, Hannover Medical School, D-30625 Hannover, Germany

[*] To whom correspondence should be addressed: Alexis De Angeli, Institute of Plant Biology, University of Zurich, Zollikerstr. 107, CH-8008 Zurich, Switzerland Tel: ++41-(0)44-6348286, Fax: ++41-(0)44-634-8204, Email: deangeli.alexis@gmail.com

**Authors e-mails:**

stmeyer@botinst uzh.ch

joachim.scholzstarke@iit.it

deangeli.alexis@gmail.com

Kovermann.Peter@mh-hannover.de

bburla@botinst.uzh.ch

gambale@ge.ibf.cnr.it

enrico.martinoia@botinst.uzh.ch

**Abbreviations:** ALMT: ALuminium activated Malate Transporter; BTP: Bis-Tris propane,

**Running title:** AtALMT6 mediates malate transport in guard cells

**Keywords:** AtALMT6, malate transport, tonoplast, guard cells, calcium-activation, *Arabidopsis thaliana*

**Total word count:** 6573

**Summary**

Gas exchange in plants is controlled by guard cells, specialized cells acting as turgor-driven valves. Malate is one of the major anions accumulated inside the vacuole during stomatal opening counteracting the positive charge of potassium. AtALMT6, a member of the aluminum-activated malate transporter family, is expressed in guard cells of leaves and stems as well as in flower organs of *Arabidopsis thaliana*. An AtALMT6-GFP fusion protein was targeted to the vacuolar membrane both in transient and stable expression systems. Patch-clamp experiments on vacuoles isolated from AtALMT6-GFP over-expressing *Arabidopsis* plants revealed large inward-rectifying malate currents only in the presence of micromolar cytosolic calcium concentrations. Further analyses showed that vacuolar pH and cytosolic malate regulate the threshold of activation of AtALMT6-mediated currents. The interplay of these two factors determines the AtALMT6 function as a malate influx or efflux channel depending on the tonoplast potential. Guard cell vacuoles isolated from *Atalmt6* knock-out plants displayed reduced malate currents compared to wild-type vacuoles. This reduction, however, was not accompanied by phenotypic differences in the stomatal movements in knock-out plants, probably because of functional redundancy of malate transporters in guard cell vacuoles.

**Introduction**

In plants, malate exhibits a multitude of functions. As an intermediate of the tricarboxylate and glyoxylate cycles it is closely linked to the production of ATP and NADH and required for β-oxidation of fatty acids. It is involved in cytosolic pH regulation and serves as a temporary storage for $CO_2$ in C4 and Crassulacean acid metabolism (CAM) plants (Fernie and Martinoia, 2009). Due to the multifunctionality of malate, its synthesis and exchange between different cellular compartments has to be tightly regulated (Martinoia and Rentsch, 1994). The fluctuation of malate concentrations is also essential for the controlled movement of guard cells. Mainly produced from starch breakdown, malate serves to balance the positive charges of potassium accumulated during stomatal opening (Roelfsema and Hedrich, 2005; Vavasseur and Raghavendra, 2005; Shimazaki *et al.*, 2007). Stomatal aperture is

controlled by light, drought, $CO_2$ concentration and air humidity and depends on several signaling components, including abscisic acid (ABA), indole-3-acetic acid (IAA) and $Ca^{2+}$ (Irving *et al.*, 1992; Lohse and Hedrich, 1992; Assmann and Shimazaki, 1999; Young *et al.*, 2006). Stomatal opening and closure are driven by the uptake or release of ions and organic metabolites leading to changes in the osmotic potential. Anionic currents carried by malate have been identified both in the plasma membrane and vacuolar membrane of guard cells, but our knowledge about the molecular identity of the respective transport systems has grown only recently. The plasma membrane-localized ABC transporter AtABCB14 catalyzes malate uptake from the apoplast into guard cells mediating stomatal opening (Lee *et al.*, 2008). The so-called R-type and S-type channels mediate anion efflux across the plasma membrane into the apoplast during stomatal closure (Keller *et al.*, 1989; Schmidt and Schroeder, 1994; Roberts, 2006). The SLAC1 (Slow Anion Channel-associated 1) protein showing homology to fungal and bacterial dicarboxylate/malic acid transporters has been identified as the channel forming protein of the S-type anion conductance (Negi *et al.*, 2008; Vahisalu *et al.*, 2008; Chen *et al.* 2010). Regarding the R-type channel component, there have been controversial results about AtALMT12 (Sasaki *et al.*, 2010; Meyer *et al.*, 2010), a member of the Aluminum-activated Malate Transporter (ALMT) family in *Arabidopsis thaliana*. While both studies agreed on the impairment of stomatal closure in loss-of-function mutants, only Meyer *et al.* (2010) found a reduction of R-type currents in these plants.

The role played by vacuolar malate channels in the control of stomatal aperture is far less characterized. Our knowledge on currents and their regulation has come for the most part from studies on mesophyll vacuoles isolated from C3 and CAM plants, rather than on guard cell vacuoles. Patch-clamp experiments have revealed anionic currents with strong inward-rectification and slow activation kinetics (Pantoja *et al.*, 1992; Hafke *et al.*, 2003). Currents in the CAM plant *Kalanchoe daigremontiana* were carried by a small-conductance ion channel (Hafke et al., 2003), whose activity increased at higher cytosolic pH values, but did not respond to changes in cytosolic calcium concentration (Pantoja and Smith, 2002). By contrast, the chloride and malate conductance identified in guard cell vacuoles of *Vicia faba* by Pei *et al.* (1996) was activated by a calcium-dependent protein kinase. Recently, the AtCLCc protein was localized in the vacuolar membrane of *Aarabidopsis thaliana*, and shown to be

involved in chloride accumulation and the regulation of stomatal movements (Jossier *et al.*, 2010). Malate transport in mesophyll vacuoles of *Arabidopsis thaliana* is accomplished by at least two transport systems, the tonoplast dicarboxylate transporter AttDT (Emmerlich et *al.*, 2003; Hurth et *al.*, 2005) and the vacuolar malate channel AtALMT9 (Kovermann *et al*., 2007). Patch-clamp measurements on the respective knock-out plants demonstrated that only AtALMT9 contributes visibly to macroscopic malate currents. Furthermore, neither mutant plant showed phenotypic differences when grown under standard conditions, indicating a high degree of functional redundancy in mesophyll vacuoles.

In this study, we were interested to fill the gap on the vacuolar malate transport system in guard cells and set out to explore whether other tonoplast-localized members of the AtALMT protein family may specifically take over this function in guard cells of *Arabidopsis thaliana*. We found that AtALMT6 was expressed in guard-cells vacuoles and is able to mediate malate inward-rectifying currents. Interestingly we observed that AtALMT6 is activated by cytosolic calcium. Cytosolic malate and vacuolar pH modulated the threshold of current activation allowing the vacuolar malate accumulation or release at physiological membrane potentials.

## Results and Discussion

### AtALMT6 is predominantly expressed in guard cells and flower tissues

In search for AtALMT protein family members expressed in *Arabidopsis* guard cells we analyzed gene expression data from microarray experiments visualized by the *Arabidopsis* eFP Browser (http://www.bar.utoronto.ca/). These data indicated strong mRNA accumulation of *AtALMT6* (At2g17470) in guard cells and also flower tissues of *Arabidopsis*. In order to verify the microarray data we transformed *Arabidopsis* plants with the *β-glucuronidase* (GUS) gene under the control of a 1.881-bp promoter region upstream of the *AtALMT6* coding sequence. Microscopic analysis of these transgenic plants revealed GUS activity in guard cells of stem and leaf epidermal cell layers (Figure 1A-D). In addition, high GUS activity was also detectable in flower tissues, e.g. sepals, petals and anthers (Figure 1E) and more weakly in leaf mesophyll cells mainly of older plants (Figure 1B). No GUS activity could be

observed in roots at any time. Taken together, our observations are largely consistent with the predicted microarray gene expression data and describe AtALMT6 as a protein with cell-type specificity in guard cells and flower tissues of *Arabidopsis*.

**AtALMT6 is localized in the vacuolar membrane**

In order to investigate the subcellular localization of the AtALMT6 protein, a construct was generated encoding the AtALMT6 protein with a C-terminal GFP fusion under the control of the *35S*-promoter. Transient expression of this construct by particle bombardment revealed that AtALMT6 was targeted to the vacuolar membrane in onion epidermal cells (Figure 2A-C). To verify these results the localization of the AtALMT6-GFP fusion construct was also studied in stably transformed *Arabidopsis* rdr6-11 plants. The genetic background of the *Arabidopsis* rdr6-11 mutant was chosen for effective suppression of endogenous gene silencing mechanisms (Peragine *et al.*, 2004). Confocal microscopy analysis of overexpressing plants showed tonoplast targeting of AtALMT6-GFP in both guard cells and isolated mesophyll vacuoles confirming the transient expression pattern (Figure 2D-G). Summarizing our localization data, AtALMT6 was identified as a member of the AtALMT protein family localized to the vacuolar membrane of *Arabidopsis* guard cells.

**AtALMT6 is a $Ca^{2+}$ activated malate channel**

In order to functionally characterize the AtALMT6 protein, we performed patch-clamp experiments on mesophyll vacuoles isolated from *Arabidopsis* rdr6-11 (WT) plants and rdr6-11 plants stably overexpressing the AtALMT6-GFP fusion construct (see above). Experiments on wild-type vacuoles revealed small currents (Figure 3A) that did not significantly respond to changes in cytosolic calcium concentration. Only at negative voltages a small time-dependent component could be observed. The current densities of this component are summarized in Figure 3C (inset). WT values were comparable to previously published data for *Arabidopsis* mesophyll vacuoles (Hurth *et al.*, 2005; Kovermann *et al.*, 2007). Vacuoles isolated from AtALMT6-GFP overexpressing plants showed bright GFP fluorescence (Figure 2F-G). The currents

recorded from these vacuoles were in most cases similar to WT currents, when the vacuoles were bathed in calcium-free solution with a very low (picomolar) free $Ca^{2+}$ concentration (Figure 3B, left). By contrast, in the presence of 100 µM $Ca^{2+}$ in the bath solution huge inward-rectifying currents were recorded (Figure 3B, right). These currents displayed a small instantaneous component (the current immediately after the voltage step, Figure 3B) and a large time-dependent component (corresponding to the relaxation after the voltage step, Figure 3B). This kinetic behaviour is reminiscent of the vacuolar malate currents recorded in *Arabidopsis* (Hurth *et al.*, 2005; Kovermann *et al.*, 2007) and in the CAM plant *Kalanchoe daigremontiana* (Hafke *et al.*, 2003). Similar current densities as detected at 100 µM free $Ca^{2+}$ were obtained already in 1 µM free $Ca^{2+}$ in the bath solution (at -100 mV: -78±41 pA/pF). Depending on the batch of protoplasts isolated from AtALMT6-GFP overexpressing plants, some variability in the calcium response was observed (see also discussion below). Some vacuoles in calcium-free bath solution occasionally displayed current density values typical of elevated $Ca^{2+}$ concentrations. On the other hand, in some vacuoles currents could not be activated by the exposure to micromolar cytosolic calcium. In both cases, vacuoles were excluded from the data sets. In order to verify whether cytosolic $Ca^{2+}$ indeed activates malate currents in AtALMT6-GFP containing vacuoles, we varied the $Ca^{2+}$ concentration of the bath solution by means of a gravity-driven perfusion system. Small malate currents in the starting condition with calcium-free solution gradually increased when the recording chamber was slowly perfused with bath solution containing 1 µM free $Ca^{2+}$ (Figure 3D). Final current densities of four vacuoles were similar to the mean values reported above (Figure 3E). In total, current increase upon exposure to elevated $Ca^{2+}$ concentrations was observed in more than ten independent vacuoles. Our data indicate that the AtALMT6-mediated malate conductance can be activated by calcium without the requirement for externally added cofactors. By contrast, the vacuolar chloride and malate conductance in *Vicia faba* guard cells reported by Pei *et al.* (1996) did not activate in response to $Ca^{2+}$ alone, but depended also on the presence of a calcium-dependent protein kinase and ATP. Vacuolar malate currents in *Kalanchoe daigremontiana* were insensitive to cytosolic $Ca^{2+}$ (Pantoja and Smith, 2002).

Interestingly, the effect of current activation could never be reversed by $Ca^{2+}$ removal, neither by prolonged slow perfusion of the recording chamber (n=10) nor by local fast perfusion with calcium-free bath solution (Figure 3F). This suggested the existence of

an irreversible step during channel activation, at least under the particular conditions of a patch-clamp experiment on an isolated vacuole. Generally speaking, a regulatory co-factor (either of cytosolic or vacuolar origin) could be removed from the channel during $Ca^{2+}$-dependent activation or alternatively could be necessary for channel inactivation. This hypothetical factor is of course present *in vivo* to promote channel closure, but is likely to be no longer available once the isolated vacuole has been perfused externally with bath solution and internally with pipette solution. For example, in *Vicia faba* guard cells, a protein phosphatase mediates stomatal opening through activation of the plasma membrane $H^+$-ATPase (Takemiya *et al.*, 2006). Furthermore, SLAC1 activation during stomatal closure is regulated by distinct protein kinases (Geiger *et al.,* 2009; Lee *et al.*, 2009; Geiger *et al.,* 2010), but depends also on protein phosphatases (Leung *et al.,* 1997; Merlot *et al.,* 2001). Moreover, the absence of a known calcium-binding motif in the AtALMT6 protein sequence lends further support to the idea that $Ca^{2+}$-dependent current activation is mediated by a yet unidentified player. Having these considerations in mind, we investigated the possibility that the AtALMT6 channel could be activated by dephosphorylation by a $Ca^{2+}$-activated protein phosphatase and, conversely, inactivated by phosphorylation. However, current activation was not suppressed in the presence of okadaic acid (300 nM), an inhibitor of protein phosphatases, in the bath solution (Supplemental Figure 1A). Moreover, addition of 2 mM ATP to calcium-free bath solution did not promote the reversal of current activation (Supplemental Figure 1B). Note that both scenarios would require that the respective enzyme (protein phosphatase or protein kinase) remains associated with the membrane of the isolated vacuole. The irreversibility of current activation provides a plausible cause for the occasional occurrence of vacuole preparations displaying high current amplitudes in the absence of $Ca^{2+}$ (see above). Malate channels may have been activated already inside mesophyll protoplasts, e.g. by elevated $[Ca^{2+}]_{cyt}$ in response to external stimuli during protoplast isolation. Nonetheless, the fact that a subset of vacuoles could not be activated in the presence of cytosolic calcium indicates that calcium is an essential but not sufficient factor for the activation of the AtALMT6-dependent current and that one or more additional factors are required for the activation of AtALMT6.

The anion selectivity of the currents observed in AtALMT6-GFP containing vacuoles was investigated by tail current analyses. With 10 mM vacuolar malate at pH 6 and

100 mM cytosolic malate at pH 7.5, the reversal potential coincided with the Nernst potential for $malate^{2-}$ and was far from reversal potential of $BTPH^{+}$, thus indicating that the current is mediated by malate anions (Figure 4A). Under the previous conditions malic acid was present mainly as $malate^{2-}$. At pH values more acidic than pH 6, malic acid is present in two different anionic species: $malate^{2-}$ and $Hmalate^{-}$ (pK 5.1). In order to verify if the AtALMT6 current discriminates between $Hmalate^{-}$ and $malate^{2-}$, we designed experiments where both species were present (Figure 4B). We used a vacuolar solution containing 130 mM malic acid at pH 4 (7.5 mM $malate^{2-}$, 97 mM $Hmalate^{-}$ and 25.5 mM $H_2$malate) and a cytosolic solution with 100 mM malate pH 7.5 (99 mM $malate^{2-}$ and 1 mM $Hmalate^{-}$). Under these conditions the reversal potential of +20±2 mV matched the Nernst potential for $malate^{2-}$ (+21 mV) and was consistently different from the Nernst potential for $malate^{-}$ (-83 mV, Figure 4B). Moreover, under different experimental conditions, including both inwardly and outwardly directed malate gradients, the reversal potential of the currents was close to the Nernst potential for $malate^{2-}$ (Figure 4C). The agreement between measured and predicted Nernst potentials for $malate^{2-}$ demonstrated that AtALMT6 behaves as an ion channel mediating the passive transport of $malate^{2-}$ across the vacuolar membrane. Moreover, this preference for a specific form of malate anions provides a basis for the channel-mediated malate accumulation in the vacuole. Next, we tested the permeability of AtALMT6-GFP mediated currents to other anions. Figure 5A shows typical current recordings of a vacuole successively challenged with bath solutions containing malate, fumarate, citrate, chloride or nitrate as the major anion. Currents recorded in the presence of fumarate were larger in amplitude, but displayed similar voltage-dependent and time-dependent activation kinetics compared to malate. In contrast, the currents with citrate, chloride or nitrate in the bath solution were about three to four times smaller than the malate currents and lacked significant voltage and time dependence. The results obtained from several vacuoles are summarized in Figure 5B and C. Higher permeability for fumarate compared to malate was also reported for the vacuolar malate conductance in *Kalanchoe daigremontiana* (Hafke *et al.*, 2003).

Summarizing, these data provided evidence that the *AtALMT6* gene encodes a vacuolar channel selective for malate and fumarate regulated by cytosolic $Ca^{2+}$ and specific for the divalent form of malate.

**Vacuolar pH and cytosolic malate regulate AtALMT6 activity**

Since it has been reported that the vacuolar pH of guard cells becomes more acidic during stomata closure (Zhang *et al.*, 2001), we wondered if $pH_{vac}$ could also directly affect AtALMT6 currents. To investigate this possibility, we imposed a defined $malate^{2-}$ gradient across the vacuolar membrane (100 $mM_{Vac}$/100 $mM_{Cyt}$) and varied the vacuolar pH (Figure 6). At vacuolar pH 6 and 7, the mean current densities at negative voltages were lower compared to the one observed at pH 5.1 (Figure 6A). Interestingly, at vacuolar pH 5.1 we observed an outward current at membrane potentials between 0 and +40 mV, corresponding to a $malate^{2-}$ release from the vacuole (Figure 6B, *inset*), followed by a tail current when the membrane potential was stepped to +60 mV. Instead, when $pH_{vac}$ 6 or 7 were applied neither time-dependent activation current at +20 mV nor tail deactivation currents at +60 mV were detected (Figure 6A). Since the substrate gradient was maintained identical in these experiments, the shift in the threshold of activation to more positive voltages induced by the vacuolar pH seems to be due to a modification of the open probability of the channel. While it was shown that cytosolic pH affects malate channel activity (Hafke *et al*. 2003; Pantoja and Smith, 2002), vacuolar pH, to our knowledge, has never been reported to affect malate currents. The shift in the activation threshold of AtALMT6 currents is intriguing since it takes place at physiological vacuolar pH.

Under the experimental conditions shown above we observed both efflux and influx of malate from and into the vacuole. Since AtALMT6 is expressed in guard cells (Figure 1), the malate fluxes mediated by this channel might be important for stomatal movements. In order to investigate a possible role in malate release during stomatal closure, we asked if outwardly directed currents could be recorded in the presence of a physiological malate gradient. For this reason, with 99 mM $malate^{2-}$ present in the patch pipette, the $malate^{2-}$ concentration in the bath solution was successively changed from 99 mM to 10 mM and further to 1 or 2 mM, shifting the Nernst potential towards negative membrane potentials (Figure 7). As expected, time-dependent inward currents appeared at more negative voltages and showed decreased amplitudes in the presence of an oppositely directed malate gradient (Figure 7). Interestingly, the tail current amplitudes, representing the outward malate currents, instead of increasing at low cytosolic $malate^{2-}$ concentrations, as one would have expected if the channel open probability remained the same, decreased. This

suggests that, at low cytosolic malate concentrations, the activation threshold of the currents is shifted to more negative voltages.

No significant outward currents (indicating malate flux out of the vacuole) could be recorded at vacuolar pH 6 (Figure 7A, C). However, with vacuolar pH 5.1 outward currents were detected at voltages more positive than the respective Nernst potential (Figure 7B, D). Specifically, at cytosolic malate concentration between 2 and 10 mM, as assumed to occur in plant cells, and at physiologically relevant membrane potentials (from -40 to 0 mV) an outward current and larger tail currents with time-dependent deactivation kinetics were observable at pH 5.1 but not at pH 6 (Figure 7 C and D, *insets*). In summary, at vacuolar pH 5.1 the negative shift of the threshold of activation induced by low cytosolic malate concentrations is counterbalanced by the positive shift induced by acidic vacuolar pH. This enables AtALMT6 to mediate malate outward currents at physiological membrane potentials. These data show that depending on the vacuolar pH and the tonoplast potential AtALMT6 can drive malate vacuolar accumulation or release. A channel-mediated accumulation of $malate^{2-}$ is able to make a $1_{cyt}/10_{vac}$ ratio at a tonoplast potential of -23 mV. However, since AtALMT6 is permeable only to $malate^{2-}$, the total amount of malic acid that can be accumulated in the vacuole is doubled when the vacuolar pH is 5.1. Therefore, the cytosolic/vacuolar malate ratio that can be reached is ~1/20 at -23 mV and ~1/50 at -40 mV.

### *Atalmt6* T-DNA mutant lines displayed reduced malate currents

Two independent *Atalmt6* mutant lines (*Atalmt6-1, Atalmt6-2*) were identified from the GABI-KAT T-DNA insertion mutant collection (*Atalmt6-1*; http://www.gabi-kat.de/; Rosso *et al*., 2003) and the Versailles *Arabidopsis* T-DNA insertion collection (*Atalmt6-2;* http://dbsgap.versailles.inra.fr/portail/; Samson *et al*., 2002), respectively.

The absence of the *AtALMT6* transcript in the mutants was demonstrated by RT-PCR (Supplemental Figure 2). As a first step to analyse the role of AtALMT6 in guard-cells we performed patch-clamp experiments on guard cell vacuoles from wild-type, *Atalmt6* mutant and overexpressing plants (Figure 8). Since *Arabidopsis* guard cell vacuoles are relatively small, we verified that we were able to control this experimental system by conducting initial patch-clamp experiments on guard cell vacuoles from AtALMT6 overexpressing plants. To avoid possible errors in the

capacitance measurements due to the small size of guard cell vacuoles (4-5 µm radius) we decided to express the currents as mere amplitude and not as current density. This approach is also justified by the homogenous size of *Arabidopsis* guard cell vacuoles. As expected, AtALMT6-GFP-containing guard cell vacuoles presented time-dependent malate currents undistinguishable from the ones measured in mesophyll vacuoles (Figure 8). The current amplitudes in the corresponding guard cell vacuoles were -890±150 pA at -100 mV (Figure 8A, B). Among six wild-type guard cell vacuoles, we found four that displayed a time-dependent malate current with an amplitude of -27±5 pA at -100 mV (Figure 8A, B). When the same experiment was carried out on *Atalmt6* mutant guard cell vacuoles we observed a time-dependent malate current of -5±2 pA at -100 mV, i.e. five times lower than the amplitude observed in wild-type vacuoles (n=5; Figure 8A, B). This ensemble of results indicates that, under our experimental conditions, AtALMT6 mediates a substantial part of the vacuolar malate current in guard cells.

The second step in the analysis of *Atalmt6* knock-out plants was to compare stomatal movements of wild-type and knock-out lines. In our experimental conditions we could not observe a clear and reproducible phenotype on the knock-out lines, neither using direct measurements of stomatal aperture in epidermal strips nor by measuring stomatal conductance in response to different stimuli with a gas exchange system (Li-Cor, www.licor.com, data not shown, Supplemental information). Mutant plants were also similar to wild-type plants in their behavior towards exposure to drought. This negative result may be explained by the residual malate currents that we observed in vacuoles isolated from knock-out guard cells. These currents could still be sufficient to mediate vacuolar malate accumulation/release and to support stomatal movements under the experimental conditions. Functional redundancy may be related to compensating mechanisms, such as the expression of other AtALMTs, the malate transporter AttDT or further anion transporters in the knock-out lines that would mask the absence of AtALMT6. RT-PCR analyses on stripped epidermal layers, however, did not reveal any obvious difference on the mRNA levels of *AtALMT9* and *AttDT* between wild-type and *Atalmt6* mutant plants (data not shown). It has also to be kept in mind that guard cells are able to make use of different anions and solutes to achieve their movements (Roelfsema and Hedrich, 2005), and that therefore, in case a vacuolar malate channel is lacking, they can still use other pathways to change their water potential.

In the present study we identified AtALMT6 as the first vacuolar malate channel of *A. thaliana* guard cells at the molecular level. Interestingly, we found that the AtALMT6 channel is activated by cytosolic calcium and modulated by vacuolar pH, two factors known to be involved in stomatal opening and closure.

While a consistent number of studies identified and characterized plasma membrane localized channels and described their respective roles in the regulation of stomatal aperture (Roelfsema and Hedrich, 2005; Ward *et al.*, 2009), to our knowledge only the vacuolar AtTPC1/SV channel, theAtTPK1/VK channel and the chloride transporter AtCLCc have been shown to affect stomatal movements (Peiter *et al.,* 2005; Gobert *et al.*, 2007, Jossier *et al.,* 2010) Further studies including other vacuolar AtALMTs and AttDT will be required to completely elucidate the role of vacuolar malate in stomatal function.

## Experimental procedures

### Strains and Growth Conditions

*Escherichia coli* (DH5α) (Hanahan, 1983) was used for cloning. *Arabidopsis thaliana* (Col-0, Ws, rdr6-11) plants were grown in controlled environment chambers in potting soil or on agar medium (8 h/16 h light/dark, 22°C, 55% relative humidity). Transformation of *Arabidopsis* was performed with *Agrobacterium tumefaciens* (GV3101) using the floral dip method according to the protocol of Clough and Bent (1998).

### Tissue specific expression and subcellular localization of *At*ALMT6 in *Arabidopsis*

A 1.881-bp promoter region upstream of *AtALMT6* was amplified from genomic DNA of *Arabidopsis* plants (Col-0) by PCR using the primers At2g17470-1881f (5′-CACCAAGCTTTTAGCAGATGATGGAAAGCAGTCG-3′) and At2g17470-1r (5′-CTAGTCTAGATTTTTCCCCTAAATTACTCTGAAGAGAACCTTTG-3′). This PCR-fragment was cloned into the *Hind*III and *Xba*I restriction sites of the vector pGPTV-

BAR (Becker *et al.*, 1992). The vector construct (pSP10a) was transformed into *Arabidopsis*, transformants were selected for Basta resistance and plants of the T2-progeny were GUS-stained at various developmental stages.

To localize *At*ALMT6 at the subcellular level, a constitutively expressed *At*ALMT6-GFP fusion protein was created. Total RNA was isolated from whole *Arabidopsis* leaves (Ws, Qiagen kit) followed by RT-PCR (Promega kit). *AtALMT6* cDNA (1.617-bp) was then amplified with the primers Mc11-forw1 (5′-CTCGAGATGGGTCCATTTCATCAGCAAAGC-3′) and Mc11-backw1 (5′-GGTACCACTTCTGCCAAAATATCTCCTAAGTC-3′) and ligated at the *Xho*I and KpnI sites at the N-terminal end of the GFP into the pGFP2 vector (Haseloff and Amos, 1995) The resulting *At*ALMT6-GFP construct (pSM9a) was transiently expressed in *Arabidopsis* and onion (*Allium cepa*) epidermal cells using a Helium Biolistic Particle Delivery system (Biorad). For stable transformation of *At*ALMT6 fused to GFP the pSM9a plasmid was digested with *Xho*I and *Eco*RI and the resulting *AtALMT6* cDNA-GFP fragment was cloned under the control of the 35S-promoter into the *Xho*I and *Eco*RI restriction sites of the 35S-10H-GFP-JH2 vector (Geisler *et al.*, 2000). The construct (pSP23a) was then transformed in *Arabidopsis* rdr6-11 mutants and transformants were selected for Basta resistance.

**Selection of *Atalmt6* knock-out lines**

Two T-DNA insertion mutant lines of *AtALMT6* (*Atalmt6-1* and *Atalmt6-2*) were identified from the GABI-KAT database (*Atalmt6-1*; GABI_259D05; http://www.gabi-kat.de/; Rosso *et al.*, 2003) and the Versailles *Arabidopsis* T-DNA insertion collection (*Atalmt6-2*; FLAG_425D02; http://dbsgap.versailles.inra.fr/portail/; Samson *et al.*, 2002), respectively. Genomic DNA was extracted from four week old plants and mutant plants homozygous for the T-DNA insertion locus were isolated by PCR genotyping using *AtALMT6* specific primers (GABI_259D05: At2g17470-GABI-LB (5′-GCATTCAGGGTGTTCTTGTTG-3′) and At2g17470-GABI-RB (5′-GATTGAATAGCGGACCTGTACC-3′); FLAG_425D02: At2g17470+1f (GAATTCATGGGTCCATTTCATCAGCAAAGC) and FLAG-LB (TGCCTTACCTCTCATGTGTGTCTG)) and T-DNA specific primers (GABI_259D05: pAC161-T-DNA LF (5′-ATATTGACCATCATACTCATTGC-3′) FLAG_425D02: LB4 (5'-CGTGTGCCAGGTGCCCACGGAATAGT-3')). The T-DNA was found to insert in the third intron of the *AtALMT6* gene in the *Atalmt6-1* mutant line and in the first

intron in the *AtALMT6-2* mutant line. Transcript analysis of *AtALMT6* in homozygous knock-out lines and WT plants was assayed by isolation of total RNA from whole leaves (Quiagen kit) followed by RT-PCR (Promega kit) using the *AtALMT6* specific primers At2g17470+1f (5′- GAATTCATGGGTCCATTTCATCAGCAAAGC-3′) and At2g17470-GABI-RB (5′- GATTGAATAGCGGACCTGTACC-3′) for both mutant lines and the control primers Actin-s (5'-TGGAATCCACGAGACAACCTA-3′) and Actin-as (5′-TTCTGTGAACGATTCCTGGAC-3′).

**Protoplast preparation and patch-clamp recordings on isolated vacuoles**

Mesophyll protoplasts were isolated as described in Scholz-Starke *et al.* (2006), with the following modifications: enzyme solution contained 0.3% (w/v) cellulase R-10, 0.03% (w/v) pectolyase Y-23, 1 mM $CaCl_2$, 500 mM sorbitol, 10 mM MES, pH 5.3. Protoplasts were washed twice and resuspended in solution without enzymes. Guard cell protoplasts were obtained using an over-night enzymatic digestion (Geiger *et al.*, 2009) and vacuoles isolated by calcium and osmotic shock.

Membrane currents of isolated vacuoles were recorded using the patch-clamp technique as described elsewhere (Scholz-Starke *et al.*, 2006). Pipette solutions contained 400 mM MES, 5 mM HCl, adjusted to pH 6.0 with 90 mM 1,3-bis[tris(hydroxymethyl)methylamino]propane (BTP) or to pH 7.0 with 210 mM BTP. The standard bath solution contained 100 mM malic acid, 160 mM BTP, 3 mM $MgCl_2$, 0.1 mM $CaCl_2$, pH 7.5. For calcium-free bath solution (0 Ca), $CaCl_2$ was omitted and 5 mM ethylene glycol-bis(2-aminoethylether)-N,N,N’,N’-tetraacetic acid (EGTA) was added. The concentration of free $Ca^{2+}$ in this solution (considering a $Ca^{2+}$ contamination of 2.5 µM measured by atomic absorption spectroscopy) was estimated to be about 20 picomolar (http://maxchelator.stanford.edu). The bath solution with 1 µM free $Ca^{2+}$ was obtained by adding 4.82 mM $CaCl_2$ to the calcium-free bath solution. For selectivity studies, malic acid in the standard bath solution was replaced by equimolar amounts of fumaric acid, citric acid, hypochloric acid and nitric acid, respectively (pH 7.5 with BTP). In experiments on vacuolar pH, the pipette solutions contained: 200 mM malic acid, 160 mM BTP, 5 mM HCl, pH 5.1; 112 mM malic acid, 100 mM BTP, 5 mM HCl, pH 6.0; 100 mM malic acid, 100 mM BTP, 5 mM HCl, pH 7.0. In experiments on outwardly directed malate currents, the pipette contained either 300 mM MES and 100 mM malic acid (pH 6.0) or 200 mM malic acid and 200 mM MES (pH 5.1), and 100 mM malate (in standard bath solution) was

replaced by 10 mM malate + 90 mM MES or 1(2) mM malate + 99 mM MES. The osmotic pressure of all solutions was 550 mosM, if necessary adjusted by addition of D-sorbitol. Ionic solutions bathing the vacuole were exchanged either by a gravity-driven perfusion system coupled to a peristaltic pump or by a local perfusion system consisting of up to five perfusion pipettes (Carpaneto *et al.*, 2001). Current-voltage characteristics were either obtained by subtracting the current at t=0 from the quasi-stationary currents (averaging the last 50 ms of the current trace) elicited by main pulses; or from the value of the tail currents (at t=0) fitted by a monoexponential function. Then current densities, plotted as pA/pF in Figs. 3-7, were obtained by normalizing the current amplitudes to the vacuole capacitance. Error bars represent standard deviation throughout the article.

Liquid junction potentials were measured according to Neher (1992). Values are given in SI text.

Ionic activities were calculated as described in SI text.

**Accession numbers**

Sequence data from this article can be found in the EMBL/GenBank datalibraries under accession number At2g17470 (AtALMT6).

**Acknowledgements**

We thank Cristiana Picco, Armando Carpaneto and Stefan Hörtensteiner for helpful discussions and suggestions. We acknowledge the financial support by the Swiss National Foundation, the German Research Foundation (JSS, SCHO 1238/1-1; SM, ME 1955/2-1), the European Molecular Biology Organisation (AD, EMBO ALTF 87-2009), EU Research Training Network Project “VaTEP” (MRTN-CT 2006-035833, FG, EM) and the Alexander von Humboldt Stiftung (PK, 1116390gadodin77). We also thank Markus Geisler for providing us with the plant binary vector p35S-GFP-JH2.

**References**

**Assmann, S.M., and Shimazaki, K.** (1999). The multisensory guard cell. Stomatal responses to blue light and abscisic acid. Plant Physiol. **119**: 809-816.

**Becker, D., Kemper, E., Schell, J., and Masterson, R.** (1992). New plant binary vectors with selectable markers located proximal to the left T-DNA border. Plant Mol. Biol. **20**: 1195-1197.

**Carpaneto, A., Cantu, A.M., and Gambale, F.** (2001). Effects of cytoplasmic $Mg^{2+}$ on slowly activating channels in isolated vacuoles of *Beta vulgaris.* Planta **213**: 457-468.

**Chen, Y-H., Hu, L., Punta, M., Bruni, R., Hillerich, B., Kloss, B., Rost, B., Love, J., Siegelbaum, S.A., and Hendrickson, W.A.** (2010). Homologue structure of the SLAC1 anion channel for closing stomata in leaves. Nature 467: 1074-1080.

**Clough, S.J., and Bent, A.F.** (1998). Floral dip, a simplified method for Agrobacterium-mediated transformation of *Arabidopsis thaliana*. Plant J. **16**: 735-743.

**Emmerlich, V., Linka, N., Reinhold, T., Hurth, M.A., Traub, M., Martinoia, E., and Neuhaus, H.E.** (2003). The plant homolog to the human sodium/dicarboxylic cotransporter is the vacuolar malate carrier. Proc. Natl. Acad. Sci. USA **100**: 11122-11126.

**Fernie, A.R., and Martinoia, E.** (2009). Malate. Jack of all trades or master of a few? Phytochemistry **70**: 828-832.

**Geiger, D., Scherzer, S., Mumm, P., Stange, A., Marten, I., Bauer, H., Ache, P., Matschi, S., Liese, A., Al-Rasheid, K.A., Romeis, T., and Hedrich, R.** (2009). Activity of guard cell anion channel SLAC1 is controlled by drought-stress signaling kinase-phosphatase pair. Proc. Natl. Acad. Sci. USA **106**: 21425-21430.

**Geiger, D., Scherzer, S., Mumm, P., Marten, I., Ache, P., Matschi, S., Liese, A., Wellmann, C., Al-Rasheid, K.A., Grill, E., Romeis, T., and Hedrich, R.** (2010). Guard cell anion channel SLAC1 is regulated by CDPK protein kinases with distinct Ca2+ affinities. Proc. Natl. Acad. Sci. USA **107**: 8023-8028.

**Geisler, M., Frangne, N., Gomès, E., Martinoia, E., and Palmgren, M.G.** (2000). The ACA4 gene of *Arabidopsis* encodes a vacuolar membrane calcium pump that improves salt tolerance in yeast. Plant Physiol. **124**: 1814-1827.

**Gobert, A., Isayenkov, S., Voelker, C., Czempinski, K., and Maathuis, F.J.** (2007). The two-pore channel TPK1 gene encodes the vacuolar K+ conductance and plays a role in K+ homeostasis. Proc. Natl. Acad. Sci. USA **104**: 10726-10731.

**Hafke, J.B., Hafke, Y., Smith, J.A., Luttge, U., and Thiel, G.** (2003). Vacuolar malate uptake is mediated by an anion-selective inward rectifier. Plant J. **35**: 116-128.

**Hanahan, D.** (1983). Studies on transformation of *Escherichia coli* with plasmids. J. Mol. Biol. **166**: 557–580.

**Haseloff, J., and Amos, B.** (1995). GFP in plants. Trends Genet. **11**: 328-329.

**Hurth, M.A., Suh, S.J., Kretzschmar, T., Geis, T., Bregante, M., Gambale, F., Martinoia, E., and Neuhaus, H.E.** (2005). Impaired pH homeostasis in *Arabidopsis* lacking the vacuolar dicarboxylate transporter and analysis of carboxylic acid transport across the tonoplast. Plant Physiol. **137**: 901-910.

**Irving, H.R., Gehring, C.A., and Parish, R.W.** (1992). Changes in cytosolic pH and calcium of guard cells precede stomatal movements. Proc. Natl. Acad. Sci. USA **89**: 1790-1794.

**Jossier, M., Kroniewicz, L., Dalmas, F., Le Thiec, D., Ephritikhine, G., Thomine, S., Barbier-Brygoo, H., Vavasseur, A., Fillieur, S., and Leonhardt, N.** (2010). The Arabidopsis vacuolar anion transporter, AtCLCc, is involved in the regulation of stomatal movements and contributes to salt tolerance. Plant J. **64**: 563-576.

**Keller, B.U., Hedrich, R., and Raschke, K.** (1989). Voltage-dependent anion channels in the plasma membrane of guard cells. Nature **341**: 250–253.

**Kovermann, P., Meyer, S., Hörtensteiner, S., Picco, C., Scholz-Starke, J., Ravera, S., Lee, Y., and Martinoia, E.** (2007). The *Arabidopsis* vacuolar malate channel is a member of the ALMT family. Plant J. **52:** 1169-1180.

**Lee, S.C., Lan, W., Buchanan, B.B., and Luan, S.** (2009). A protein kinase-phosphatase pair interacts with an ion channel to regulate ABA signaling in plant guard cells. Proc. Natl. Acad. Sci. USA **106**: 21419-21424.

**Lee, M., Choi, Y., Burla, B., Kim, Y.Y., Jeon, B., Maeshima, M., Yoo, J.Y., Martinoia, E. and Lee, Y.** *(*2008). The ABC transporter AtABCB14 is a malate importer and modulates stomatal response to $CO_2$. Nat. Cell Biol. **10:** 1217-1223.

**Leung, J., Merlot, S., and Giraudat, J.** (1997). The *Arabidopsis* ABSCISIC ACID-INSENSITIVE2 (ABI2) and ABI1 genes encode homologous protein phosphatases 2C involved in abscisic acid signal transduction. Plant Cell **9:** 759-771.

**Lohse, G., and Hedrich, R.** (1992). Characterization of the plasma-membrane $H^+$ ATPase from *Vicia faba* guard cells. Planta **188:** 206-214.

**Martinoia, E., and Rentsch, D.** (1994). Malate Compartmentation-Responses to a Complex Metabolism. Annu. Rev. Plant Physiol. Plant Mol. Biol. **45:** 447-467.

**Merlot, S., Gosti, F., Guerrier, D., Vavasseur, A., and Giraudat, J.** (2001). The ABI1 and ABI2 protein phosphatases 2C act in a negative feedback regulatory loop of the abscisic acid signalling pathway. Plant J. **25**: 295-303.

**Meyer, S., Mumm, P., Imes, D., Endler, A., Weder, B., Al-Rasheid, K.A., Geiger, D., Marten, I., Martinoia, E., and Hedrich, R.** (2010). AtALMT12 represents an R-type anion channel required for stomatal movement in Arabidopsis guard cells. Plant J. **63**: 1054-1062.

**Negi, J., Matsuda, O., Nagasawa, T., Oba, Y., Takahashi, H., Kawai-Yamada, M., Uchimiya, H., Hashimoto, M., and Iba, K.** (2008). $CO_2$ regulator SLAC1 and its homologues are essential for anion homeostasis in plant cells. Nature **452**: 483-486.

**Neher, E.** (1992). Correction for liquid junction potentials in patch clamp experiments. Methods Enzymol. **207:** 123-131.

**Pantoja, O., Gelli, A., and Blumwald, E.** (1992). Characterization of Vacuolar Malate and K Channels under Physiological Conditions. Plant Physiol. **100**:1137-41.

**Pantoja, O., and Smith, J.A.** (2002). Sensitivity of the plant vacuolar malate channel to pH, $Ca^{2+}$ and anion-channel blockers. J. Membr. Biol. **186**: 31-42.

**Pei, Z.M., Ward, J.M., Harper, J.F., and Schroeder, J.I.** (1996). A novel chloride channel in *Vicia faba* guard cell vacuoles activated by the serine/threonine kinase, CDPK. EMBO J. **15**: 6564-6574.

**Peiter, E., Maathuis, F.J., Mills, L.N., Knight, H., Pelloux, J., Hetherington, A.M., and Sanders, D.** (2005). The vacuolar $Ca^{2+}$-activated channel TPC1 regulates germination and stomatal movement. Nature **434**: 404-408.

**Peragine, A., Yoshikawa, M., Wu, G., Albrecht, H.L., and Poethig, R.S.** (2004). SGS3 and SGS2/SDE1/RDR6 are required for juvenile development and the production of trans-acting siRNAs in *Arabidopsis*. Genes Dev. **18**: 2368-2379.

**Roberts, S.K.** (2006). Plasma membrane anion channels in higher plants and their putative functions in roots. New Phytol. **169**: 647-666.

**Roelfsema, M.R., and Hedrich, R.** (2005). In the light of stomatal opening: new insights into 'the Watergate'. New Phytol. **167:** 665-691.

**Rosso, M.G., Li, Y., Strizhov, N., Reiss, B., Dekker, K., and Weisshaar, B.** (2003). An *Arabidopsis thaliana* T-DNA mutagenized population (GABI-Kat) for flanking sequence tag-based reverse genetics. Plant Mol. Biol. **53**: 247-259.

**Samson, F., Brunaud, V., Balzergue, S., Dubreucq, B., Lepiniec, L., Pelletier, G., Caboche, M., and Lecharny, A.** (2002). FLAGdb/FST: a database of mapped flanking insertion sites (FSTs) of *Arabidopsis thaliana* T-DNA transformants. Nucleic Acids Res. **30**: 94-97.

**Sasaki, T., Mori, I.C., Furuichi, T., Munemasa, S., Toyooka, K., Matsuoka, K., Murata, Y., and Yamamoto, Y.** (2010). Closing plant stomata requires a homolog of an aluminum-activated malate transporter. Plant Cell Physiol. **51**: 354-365.

**Shimazaki, K., Doi, M., Assmann, S.M., and Kinoshita, T.** (2007). Light regulation of stomatal movement. Annu. Rev. Plant Biol. **58**: 219-247.

**Schmidt, C., and Schroeder, J.I.** (1994). Anion selectivity of slow anion channels in the plasma membrane of guard cells (large nitrate permeability). Plant Physiol. **106**: 383–391.

**Scholz-Starke, J., Carpaneto, A., and Gambale, F.** (2006). On the interaction of neomycin with the slow vacuolar channel of *Arabidopsis thaliana*. J. Gen. Physiol. **127**: 329-340.

**Takemiya, A., Kinoshita, T., Asanuma, M., and Shimazaki, K.** (2006). Protein phosphatase 1 positively regulates stomatal opening in response to blue light in *Vicia faba*. Proc. Natl. Acad. Sci. USA **103**: 13549-13554.

**Vahisalu, T., Kollist, H., Wang, Y.F., Nishimura, N., Chan, W.Y., Valerio, G., Lamminmäki, A., Brosché, M., Moldau, H., Desikan, R., Schroeder, J.I., and Kangasjärvi, J.** (2008). SLAC1 is required for plant guard cell S-type anion channel function in stomatal signalling. Nature **452**: 487-491.

**Vavasseur, A., and Raghavendra, A.S.** (2005). Guard cell metabolism and $CO_2$ sensing. New Phytol. **165**: 665-682.

**Ward, J.M., Mäser, P., and Schroeder, J.I.** (2009). Plant ion channels: gene families, physiology, and functional genomics analyses. Annu. Rev. Physiol. **71**: 59-82.

**Young, J.J., Mehta, S., Israelsson, M., Godoski, J., Grill, E., and Schroeder, J.I.** (2006). $CO_2$ signaling in guard cells, calcium sensitivity response modulation, a $Ca^{2+}$-independent phase, and $CO_2$ insensitivity of the gca2 mutant. Proc. Natl. Acad. Sci. USA **103**: 7506-7511.

**Zhang, X., Dong, F.C., Gao F.J., and Song, C.P.** (2001). Hydrogen peroxide-induced changes in intracellular pH of guard cells precede stomatal closure. Cell Research **11:** 37–43.

**Supporting information**

**Supporting Experimental procedures**

**Supplemental Figure 1.** Calcium-dependent AtALMT6 current activation is not suppressed in the presence of okadaic acid and not reversed in the presence of ATP.

**Supplemental Figure 2.** Transcriptional analysis of the *Atalmt6* knock-out lines.

**Figure Legends**

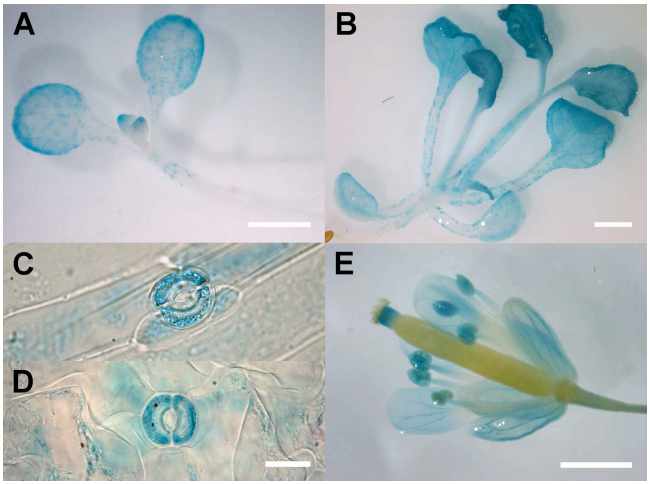


**Figure 1.** Analysis of *At*ALMT6 expression by *AtALMT6 promoter:GUS* reporter plants.

**(A)** *Arabidopsis* plants (8 days after germination) showing GUS activity mainly in guard cells of leaves and stems (marked by an arrow).

**(B)** *Arabidopsis* plants (21 days after germination) showing GUS activity in guard cells of leaves and stems and more weakly in the leaf mesophyll tissue.

**(C)** and **(D)** Close-up of stem **(C)** and leaf **(D)** guard cells.

**(E)** GUS activity in *Arabidopsis* flower tissues.

Scale bars: 1 mm in **(A)** and **(B)**; 25 µm in **(C)** and **(D)**; 0.5 mm in **(E)**.

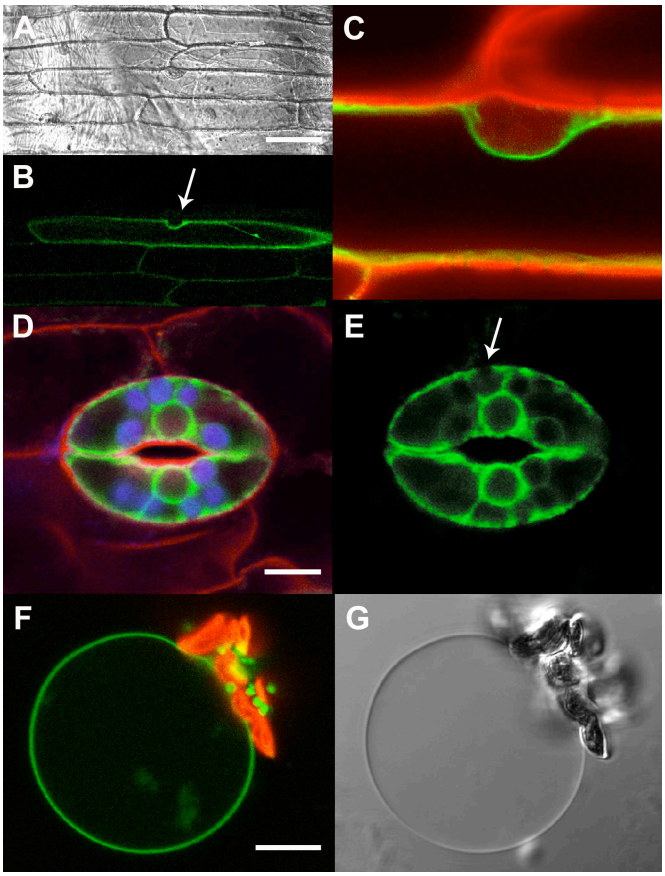


**Figure 2.** Subcellular localization of AtALMT6 by transient and stable expression of an AtALMT6-GFP fusion protein.

**(A)** to **(C)** In onion epidermal cells the AtALMT6-GFP fusion protein is targeted to the tonoplast (nucleus marked by an arrow in **(B)**). The detailed picture **(C)** shows the same onion epidermal cell as in the image **(A)** and **(B)** (Cell walls and nuclei were stained red with propidium iodide).

**(D)** and **(E)** In chloroplast-containing guard cells of stably transformed *Arabidopsis* plants the AtALMT6-GFP fusion protein is also localized to the tonoplast (chloroplasts are shown in blue, cell walls were stained red with propidium iodide in picture **(D)**). The GFP fluorescence surrounds the chloroplast (marked by an arrow) **(E)** located in the cytoplasm between the vacuole and the plasma membrane of the cell.

**(F)** and **(G)** Fluorescence **(F)** and transmission **(G)** picture of a vacuole isolated from an *Arabidopsis* mesophyll protoplast overexpressing AtALMT6-GFP (chloroplasts show red auto fluorescence). Scale bars: 50 µm in **(A)**; 10 µm in **(D)** to **(F)**.

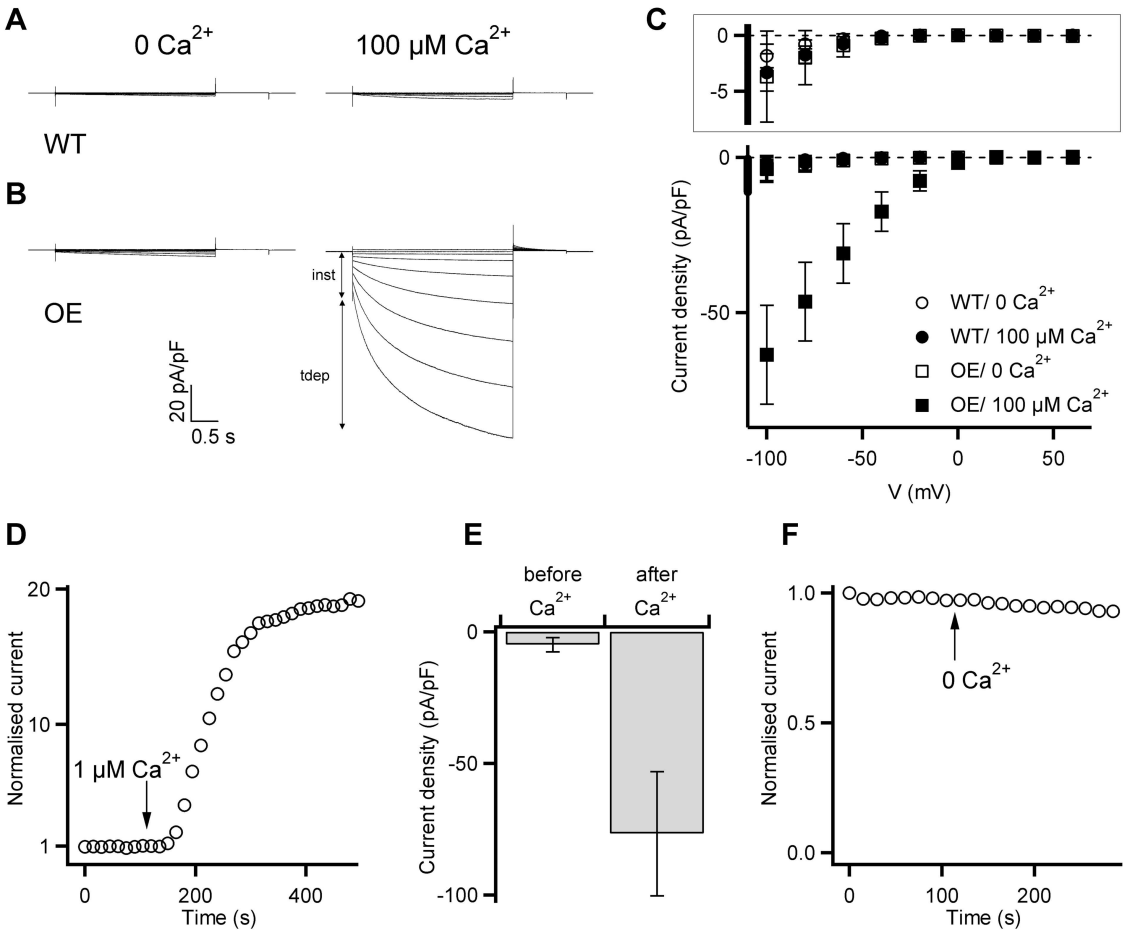


**Figure 3.** High malate currents in vacuoles from AtALMT6-GFP overexpressing *Arabidopsis* plants at micromolar cytosolic $Ca^{2+}$.**(A)** and **(B)** Whole-vacuolar current responses of vacuoles isolated from **(A)** wild-type (WT) and **(B)** AtALMT6-GFP overexpressing *Arabidopsis* plants (OE) recorded in the nominal absence of calcium (0 $Ca^{2+}$; left) and in the presence of 100 µM $Ca^{2+}$ (right) in the bath solution. From a holding potential of 0 mV (0 $Ca^{2+}$) or +40 mV (100 µM $Ca^{2+}$), a series of test voltages from +60 to –100 mV in steps of 20 mV was applied; tail potential +50 mV. Current amplitudes were normalised to the membrane capacitance. The arrows in (**B**) show the instantaneous (*inst*) and time-dependent (*tdep*) components relative to the trace at -100 mV, respectively.**(C)** Current-voltage relationships of experiments performed as in **(A)** and **(B)**. Mean time-dependent current densities are plotted as a function of the applied membrane potential (see Materials and methods). For clarity, the range of small current values has been expanded in the inset (top). **(D)** Time course of the $Ca^{2+}$-induced increase of time-dependent currents. At the time point indicated by the arrow, calcium-free bath solution was gradually substituted by bath solution containing 1 µM free $Ca^{2+}$ (by slow perfusion of the recording chamber). Currents were normalised to the value at t=0 s. Test potential -80 mV. **(E)** Mean time-dependent current density values of four different vacuoles recorded first in calcium-free bath solution (before) and subsequently in bath solution containing 1 µM free $Ca^{2+}$ (after). Test potential -100 mV.**(F)** Time-dependent currents recorded from a vacuole (representative of a total of 3) initially exposed to bath solution containing 1 µM free $Ca^{2+}$ and subsequently to calcium-free bath solution. Local perfusion allowed the immediate change of solutions (indicated by the arrow). Currents were normalised to the value at t=0 s. Test potential -80 mV.

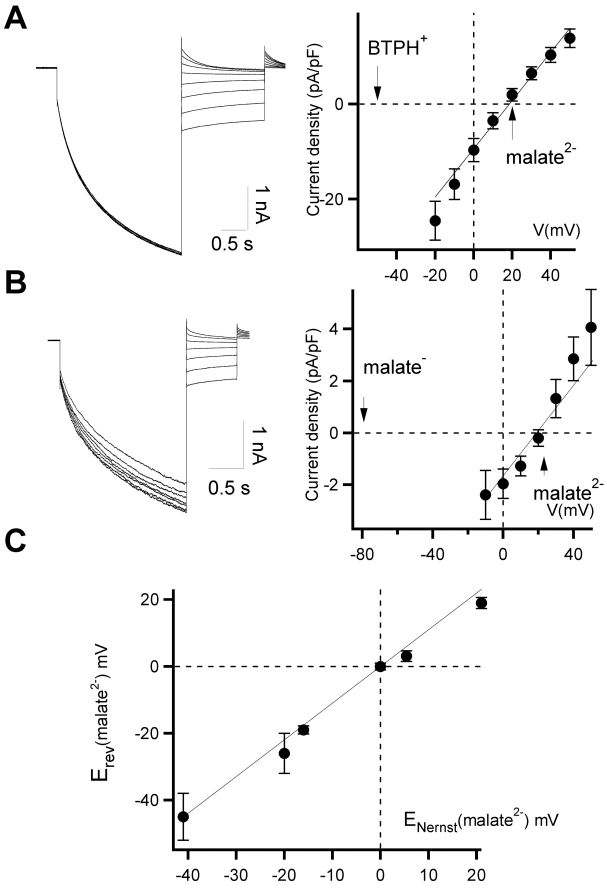


**Figure 4.** Malate currents from AtALMT6-GFP overexpressing plants display malate$^{2-}$ selectivity.
**(A)** and **(B)** *left panels,* show representative tail current recordings elicited by a series of test pulses between –20 and +50 mV (in steps of 10 mV) following an activating pre-pulse at –80 mV from a holding potential of +60 mV. In **(A)** recordings were done in the whole-vacuole configuration with 99 mM malate$^{2-}$ (standard bath solution, pH 7.5) on the cytosolic membrane side and 9 mM malate$^{2-}$ (pH 6.0) on the vacuolar side. In **(B)** recordings were done in the whole-vacuole configuration with 99 mM malate$^{2-}$ and 1 mM Hmalate$^{-}$ (standard bath solution, pH 7.5) on the cytosolic membrane side and 8 mM malate$^{2-}$ and 98 mM Hmalate$^{-}$ (pH 4.0) on the vacuolar side. The *right panels* in **(A)** and **(B)** display the mean current-voltage relationships of instantaneous tail currents recorded from 4 different vacuoles. Instantaneous tail current values were obtained from a monoexponential fit of tail current traces, normalised to the vacuolar membrane capacitance and averaged. Data points were subjected to a weighted linear fit. In **(A)** the reversal potential of +19±4 mV overlaps to the Nernst potential for malate$^{2-}$ (+21 mV) and is far from the Nernst potential for BTPH$^{+}$ (-50 mV), the major cation in the experimental solutions. In **(B)** the reversal potential was +20±2 mV that also approaches the Nernst potential for malate$^{2-}$ (+21 mV) while it is far from the Nernst potential for Hmalate$^{-}$ (-83 mV).
**(C)** Plot of the theoretical Nernst potential for malate$^{2-}$ versus observed reversal potentials in different ionic conditions. The linear fit of the data points presents a slope of 1.09±0.06.

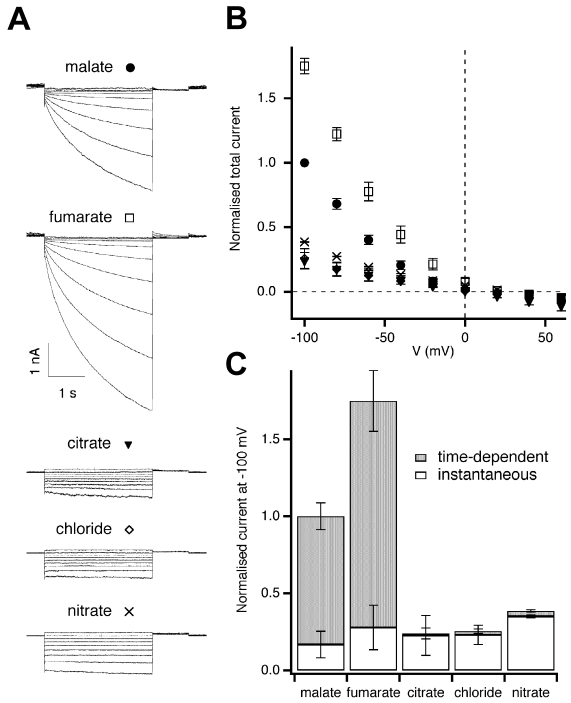


**Figure 5.** Anion selectivity of AtALMT6-GFP currents.

**(A)** Mesophyll vacuoles isolated from an AtALMT6-GFP overexpressing plant were successively exposed to different bath solutions containing 100 mM of the indicated anion (general composition of standard bath solution). The pipette solution contained 10 mM malate (pH 7.0). Representative whole-vacuolar current traces recorded upon voltage stimulation from +60 to –100 mV. The holding potential was +40 mV, the tail potential +50 mV.

**(B)** Normalised total currents recorded in the five different bath solutions (symbols as in **(A)**) are plotted as a function of the applied membrane potential. For every single vacuole, total current values (taken at the end of the voltage pulse) were normalised to the respective malate current value at +100 mV. Normalised currents for every condition were averaged (n = 9 for malate, 4 for fumarate, 6 for chloride, 3 for citrate and nitrate).

**(C)** Bar plot illustrating the relative contributions of instantaneous and time-dependent components to the total currents recorded at +100 mV in **(B)**.

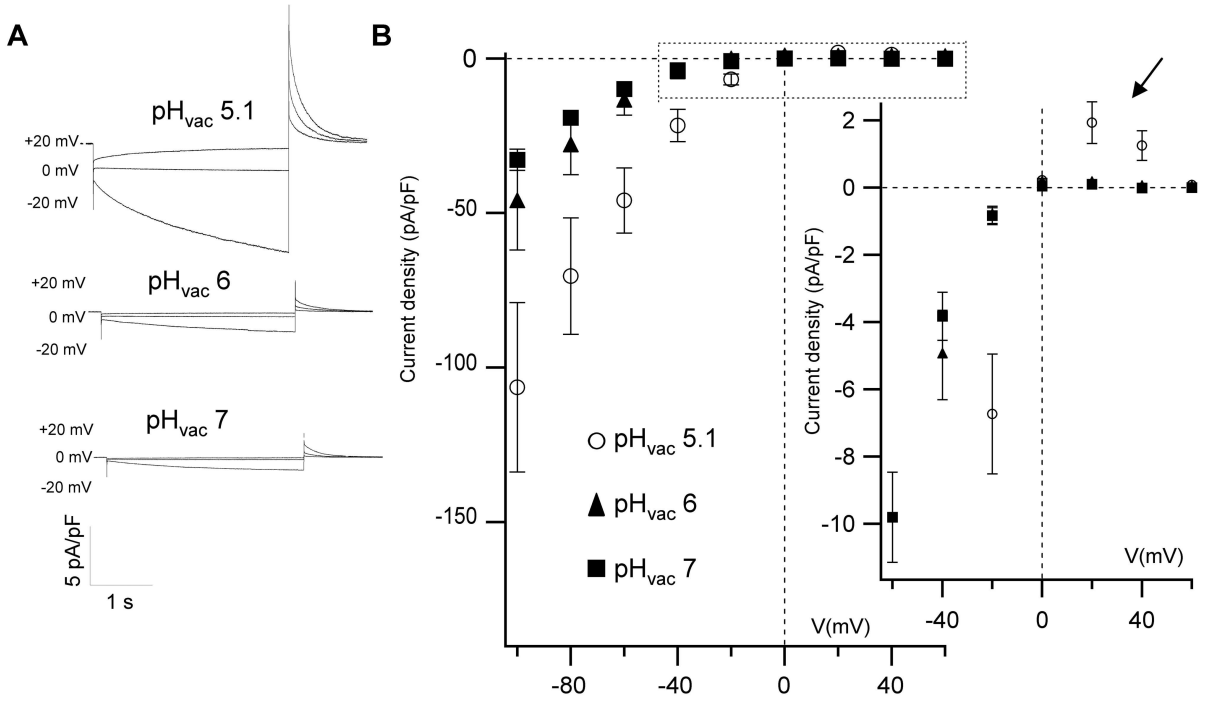


**Figure 6.** The vacuolar pH modulates the voltage dependence of AtALMT6-GFP currents.

**(A)** Representative current responses recorded from mesophyll vacuoles from AtALMT6-GFP overexpressing *Arabidopsis* plants at different vacuolar pHs. From a holding potential of +60 mV test voltages from +20 to –20 mV in steps of 20 mV were applied; the tail potential was +60 mV.

**(B)** Current-voltage relationship of AtALMT6-mediated currents in the presence of different vacuolar pHs: 5.1, 6 and 7. Average time-dependent current densities are plotted as a function of the applied membrane potential. The cytosolic solution was the standard bath solution, and the vacuolar solutions were prepared in order to keep the malate$^{2-}$ gradient to $100_{vac}/100_{cyt}$ (i.e. $E_{rev}$=0 mV) in the three conditions. At vacuolar pH 5.1 and membrane potentials ranging between 0 mV and +60 mV, outward malate$^{2-}$ currents (indicated by the arrow in the inset) are visible (*inset*).

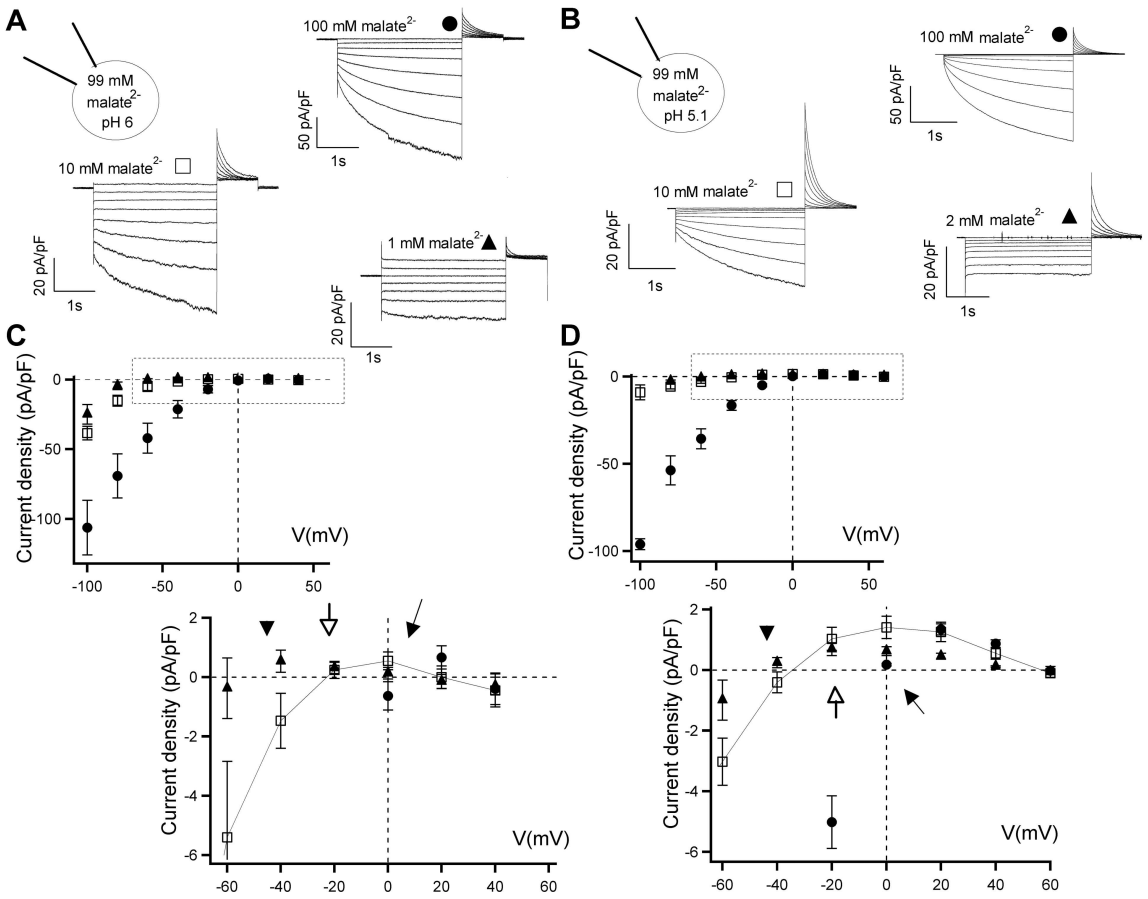


**Figure 7.** The cytosolic malate concentration influences the voltage-dependence of AtALMT6-GFP currents.

**(A)** and **(B)** representative current responses of mesophyll vacuoles isolated from AtALMT6-GFP overexpressing *Arabidopsis* plants recorded in the presence of 100 mM (*top*), 10 mM (*left*) or 1 (2) mM $malate^{2-}$ (*right*) in the bath solution. The pipette solution contained **(A)** 99 mM $malate^{2-}$ pH 6.0, **(B)** 99 mM $malate^{2-}$ pH 5.1. At vacuolar pH 5.1 and 2 /10 mM cytosolic $malate^{2-}$ **(B)** large tail current with time-dependent deactivation kinetics were recorded compared to equivalent conditions at vacuolar pH 6 **(A)**. **(C)** and **(D)** current-voltage relationships from experiments performed as in **(A)** and **(B)**. Average time-dependent current densities are plotted as a function of the applied membrane potential. (inset: I-V relationship at larger current density resolution). Theoretical Nernst potentials are indicated: $mal_{cyt}$/ $mal_{vac}$ 100/100, 0 mV (*arrow*); 10/100, -20 mV (*empty arrow*); 1(2)/100, -42 mV (*arrow-head*). The comparison of the *insets* in **(C)** and **(D)** shows that only in presence of pH 5.1 an outward $malate^{2-}$ current is observable at membrane potentials between -20 mV and +40 mV with $mal_{cyt}$/$mal_{vac}$ 10/100 and 2/100. From a holding potential of +40/+60 mV, a series of test voltages from +40/+60 to –100 mV in steps of 20 mV was applied; the tail potential was +50 mV. Time-dependent current amplitudes were normalised to the membrane capacitance.

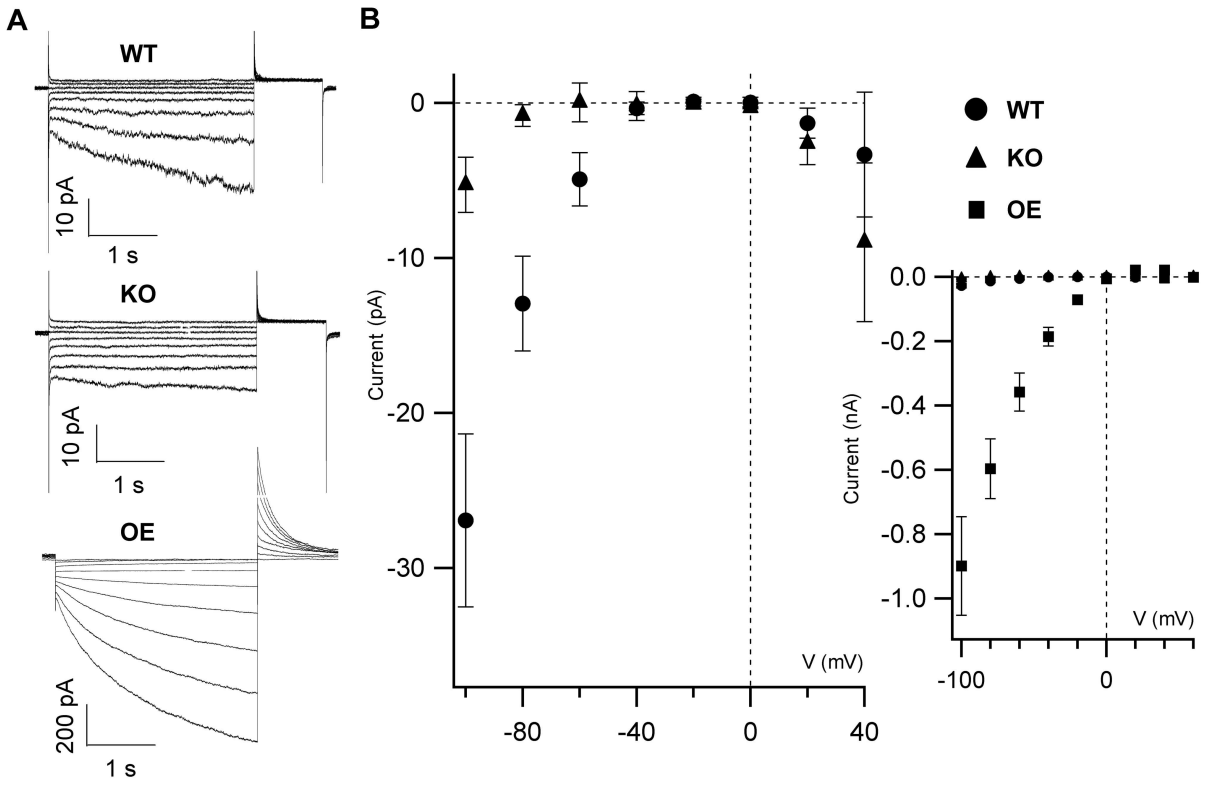


**Figure 8.** Reduced malate current amplitudes in guard-cell vacuoles from *Atalmt6* knock-out plants.

**(A)** Representative malate currents evoked in vacuoles extracted from guard-cell protoplasts isolated from wild-type (WT), *Ataltm6-1* knock-out (KO) and AtALMT6-GFP overexpressing (OE) *Arabidopsis* plants. The currents where recorded in the presence of 100 mM $malate^{2-}$ and 0.1 mM $CaCl_2$ in the cytosolic solution (standard bath solution) and the vacuolar solution contained 100 mM $malate^{2-}$ pH 5.1. From a holding potential of +40/+60 mV, a series of test voltages from +60 to –100 mV in steps of 20 mV was applied; the tail potential was +60 mV.

**(B)** Current-voltage relationships of the time-dependent current from experiments performed as in **(A)**. At voltages between -100 and -60 mV, wild-type vacuoles presented 5 to 3 times higher current amplitudes compared to knock-out vacuoles, respectively. The malate current amplitude in guard-cell vacuoles from overexpressing plants (*inset*) was far higher compared to the wild-type plants. The time-dependent current amplitudes were averaged from n=4 (WT); n=5 (KO); n=6 (OE) experiments.

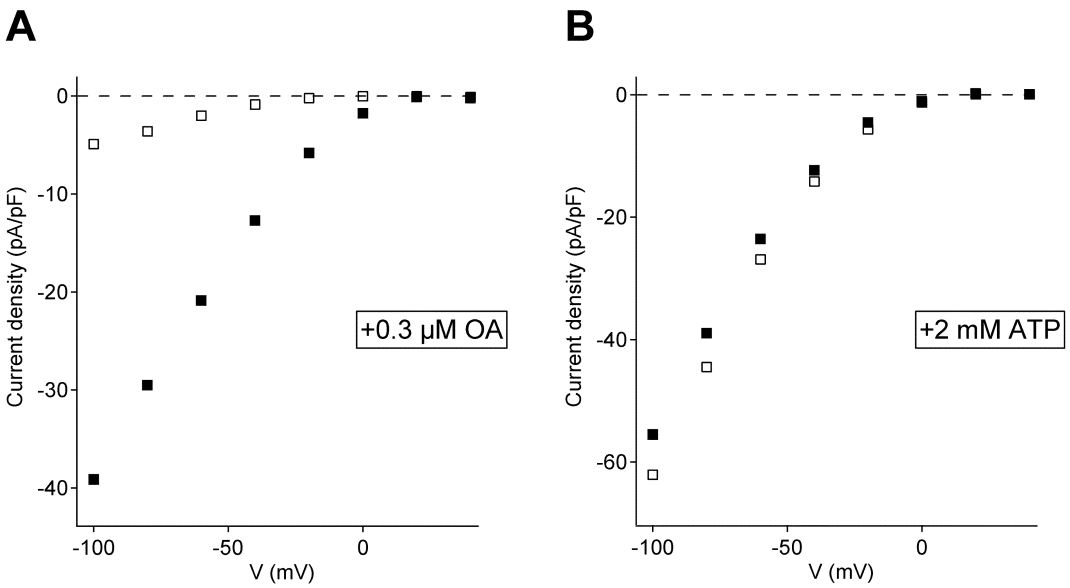


**Supplemental Figure 1:** Calcium-dependent AtALMT6 current activation is not suppressed in the presence of okadaic acid and not reversed in the presence of ATP. **(A)** Current-voltage relationships of a representative experiment performed as in Figure 3**(D)**, but in the presence of 0.3 µM okadaic acid (OA). Whole-vacuolar current responses were recorded from an AtALMT6-GFP-containing vacuole. Timedependent current densities in the starting condition with 0 Ca plus OA and after perfusion of the recording chamber with bath solution containing 100 µM Ca2+ plus OA are plotted as a function of the applied membrane potential.
**(B)** Current-voltage relationships of a representative experiment performed as in Figure 3**(F)**, but in the presence of 2 mM ATP-Mg. Whole-vacuolar current responses were recorded from an AtALMT6-GFP-containing vacuole. Time-dependent current densities in the starting condition with 100 µM Ca2+ plus ATP and after perfusion of the recording chamber with calcium-free bath solution plus ATP are plotted as a function of the applied membrane potential.
Experiments were conducted in 3 replicates. Open symbols represent the respective starting condition; closed symbols represent the test condition.

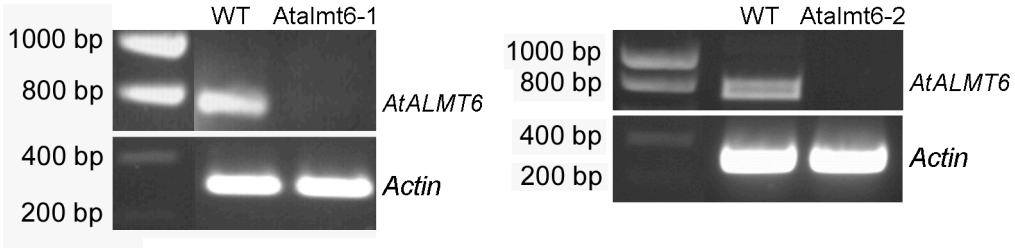


**Supplemental Figure 2.** Transcriptional analysis of the *Atalmt6* knock-out lines. Semi-quantitative RT-PCR analysis demonstrated the lack of *AtALMT6* transcript in the homozygous T-DNA mutant lines *AtALMT6-1* and *AtALMT6-2.*